Performance Tradeoffs in MEMS Sensors with High-Finesse Fabry-Perot Interferometry Detection

E. Jesper Eklund and Andrei M. Shkel

Microsystems Laboratory, University of California, Irvine, USA
eeklund@uci.edu, ashkel@uci.edu

ABSTRACT

A detailed analysis with experimental verification of optical sensors based on Fabry-Perot interferometers is presented. This type of sensor consists of two partially transparent parallel plates with reflective inner surfaces, forming a cavity with an optical resonance that depends on the distance between the plates. At resonant wavelengths, the incident light energy is transmitted through the device and intensity peaks occur. The distance between the plates can be obtained by detecting the wavelength of the transmitted light. Various optical sensors can be based on this concept, e.g. accelerometers, pressure sensors, and microphones. This paper considers factors affecting the performance of such sensors, including mechanical-thermal noise, contribution of noise in the detection system, and effects of reflectivity, surface roughness and parallelism of the mirrors.

Keywords: optical sensors, MOEMS, Fabry-Perot interferometers

1 INTRODUCTION

Optical detection systems based on Fabry-Perot interferometry allow for highly sensitive sensors, potentially detecting displacements on a sub-nanometer scale. A Fabry-Perot interferometer (FPI) consists of two parallel mirrors, which define a cavity with an optical resonance that depends on the distance between the mirrors. At resonance, the incident light energy is transmitted through the FPI, forming transmission intensity peaks at the resonant wavelengths. Despite the simplicity of Fabry-Perot interferometers, these devices offer seemingly endless possibilities. In addition to the many applications in optical communications, a wide range of sensors can be based on FPI-principles. An FPI with a suspended mirror can be used as the sensing element of accelerometers, microphones, and pressure sensors, as illustrated in Fig. 1.

The sensor node itself does not use electrical power, making this type of sensor ideal for robust devices resistant to electromagnetic interference (EMI) and radio frequency interference (RFI). Furthermore, FPI-based sensors can be serialized in a linear network by connecting multiple passive sensors between a central light source and a single detection system [1]. These devices are also promising candidates for biomedical applications, since no electrical signal is required in the sensor node.

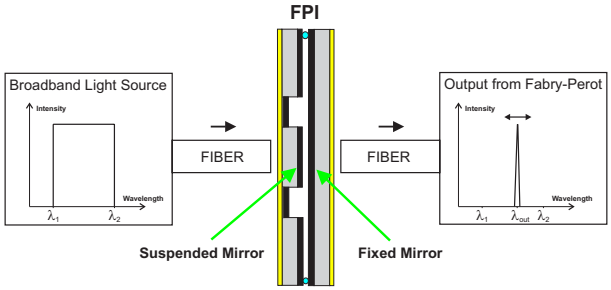

Figure 1: Fabry-Perot interferometer sensor concept.

Along with the advantages offered by this type of optical detection schemes, there are many design tradeoffs. Some of the issues that need to be considered are mechanical-thermal noise, electrical noise in the detection system, effects of reflectivity, surface roughness and parallelism of the mirrors, assembly, and packaging. The design considerations and tradeoffs of Fabry-Perot interferometers are discussed in this paper and the theoretical performance limitations are compared to experimental results obtained from an FPI-prototype.

2 FPI PRINCIPLE

Two parallel plates with reflective inner surfaces form a Fabry-Perot interferometer, which can serve as the main building block of an optical sensor. If light with a wide wavelength spectrum is transmitted through the FPI, the intensity of the transmitted light at a particular wavelength depends on the distance between the plates, d, according to the Airy function:

$$\tau = \frac{T^2}{(1-R)^2}\left[1+\frac{4R}{(1-R)^2}\sin^2\left(\frac{2\pi n d\cos\theta}{\lambda}\right)\right]^{-1}, \quad (1)$$

where R is the reflectivity of the mirrors, T is the transmission, n is the refractive index, θ is the angle of incidence, and λ is the wavelength [2]. As can be noted from equation (1), the maximum intensity will occur when $\sin^2(2\pi n d\cos\theta/\lambda) = 0$. The plate distance that

will generate an intensity peak is therefore

$$d = \frac{m\lambda}{2ncos\theta}, \tag{2}$$

where m specifies the order of interference.

In order to measure the deflection of a sensor, e.g. due to acceleration or pressure, a relationship between deflection and wavelength needs to be derived. Assume the angle of incidence of the light and the refractive index of the medium remain constant. If (2) is differentiated, $\Delta d = \Delta\lambda d_0/\lambda_0$ can be obtained, where d_0 is the initial cavity gap, λ_0 is the wavelength that generates a peak at d_0, Δd is the change in plate spacing due to acceleration or pressure, and $\Delta\lambda$ is the shift in wavelength due to Δd. For example, the response of a quasi-static accelerometer is $a = \omega_n^2 \Delta d$, where ω_n is the natural frequency. By utilizing equation (2), a direct relationship between measured acceleration and shift in wavelength of the intensity peak, $\Delta\lambda$, can be obtained as

$$a = \frac{m\omega_n^2}{2ncos\theta}\Delta\lambda. \tag{3}$$

Equation (3) shows that the resolution is affected by the natural frequency, order of interference, refractive index, and angle of incidence of the light. In a highly sensitive accelerometer, a small acceleration should cause a large shift in wavelength. Thus, both the order of interference and natural frequency need to be limited.

2.1 Finesse

The quality of a Fabry-Perot interferometer can be determined by its finesse, which is defined as the distance between the interference peaks, or free spectral range (FSR), divided by the full width half maximum (FWHM) of the peaks. In other words, the finesse is a measurement of how many peaks at FWHM the FPI can be tuned over without encountering the next order fringe and cause an ambiguous output. The finesse depends solely on the mirror reflectivity in an ideal FPI [2]:

$$N_R = \frac{\pi\sqrt{R}}{1-R}. \tag{4}$$

However, fabrication imperfections will reduce the finesse of Fabry-Perot interferometers. These effects were described in [2], where spherical bowing δt_S, surface roughness (root-mean-square deviation) δt_G, and departure from parallelism δt_P were considered. If all three defects are included, the overall defect finesse N_D, at a particular wavelength λ, is determined from

$$\frac{1}{N_D^2} = \left(\frac{2\delta t_S}{\lambda}\right)^2 + \left(\frac{4.7\delta t_G}{\lambda}\right)^2 + \left(\frac{\sqrt{3}\delta t_P}{\lambda}\right)^2. \tag{5}$$

If the defects are considered together with the reflection finesse, an effective finesse, N_E, is defined by

$$\frac{1}{N_E^2} = \frac{1}{N_D^2} + \frac{1}{N_R^2}. \tag{6}$$

2.2 Light Source and Detection Scheme

Several different systems can be considered in order to detect the wavelengths transmitted by the Fabry-Perot interferometer. A fairly simple system consists of a laser diode and a single photodiode. In order to achieve an approximately linear output with this system, only a small part of the transmission curve can be used. This limits the possible deflection of the proof mass and in turn the range of the sensor. One advantage of utilizing this detection system is that the FPI and photodiode can potentially be integrated on a single chip, as reported in [3].

An alternative way of detecting the wavelength shift is to sweep the wavelengths of a tunable laser, as shown in Fig. 2. Once the signal is transmitted through the FPI, a photodiode is used to detect the intensity peaks. Due to the limited sweeping rate of tunable lasers, this system can only operate at low frequencies. However, a high-frequency tunable FPI can potentially be implemented to achieve higher sweeping frequency.

Figure 2: Tunable laser and single photodiode detection.

As illustrated in Fig. 3, a broadband light source with a wide wavelength spectrum can be utilized. The light is optically demodulated with a diffraction grating and directed onto a linear photodiode array, and the position where the light hits the array can be related to the plate spacing. By utilizing this type of system, the full spectral range of an FPI-sensor can be utilized.

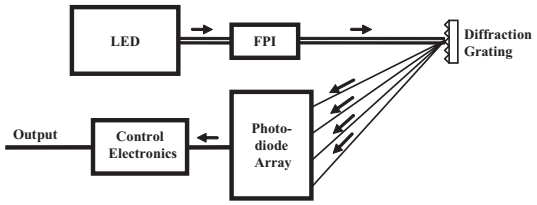

Figure 3: Detection system consisting of a diffraction grating and photodiode array.

3 NOISE

In addition to the finesse and detection system, discussed in the previous sections, other factors that affect the sensor performance are the mechanical-thermal noise and photodetector noise.

3.1 Mechanical-Thermal Noise

Mechanical-thermal noise can be estimated from the Equipartition theorem or Nyquist relation [4]. As an example, consider the accelerometer response $|H(f)|$, which leads to a Nyquist noise displacement of

$$\frac{|X_n(f)|}{\sqrt{\Delta f}} = \sqrt{4k_bTb}\frac{|H(f)|}{k}, \quad (7)$$

where k_B is Boltzmann's constant, T is the temperature, b is the damping, and k is the equivalent spring constant.

Following [4], the signal response of an accelerometer can be written as $|X_s(f)| = (f/f_n)^2 |H(f)||Y_s|$, where $\omega^2|Y_s|$ is the magnitude of the input acceleration in meters per square second per root hertz. The signal response is $|X_s(f)|/\sqrt{\Delta f} = a|H(f)|/\omega_n^2$, and the signal-to-noise ratio (SNR) of the displacement is

$$\left|\frac{X_s}{X_n}\right|^2 = \frac{a^2M}{8k_BT\xi\omega_n}, \quad (8)$$

where b has been replaced by the damping ratio $\xi = b/(2M\omega_n)$, and M is the mass. By setting $|X_s/X_n| = 1$, the smallest detectable acceleration can be obtained. For example, assume a cylindrical proof mass with radius $200\mu m$ is defined in a $500\mu m$ thick silicon wafer. Assuming critical damping ($\xi \approx 0.7$), the noise equivalent resolution is calculated to be $8\mu G$. Better resolution can be obtained if an under-damped accelerometer is designed by vacuum packaging the device or increasing the plate spacing. However, as discussed in Section 2, an increased spacing yields a higher order of interference. This reduces the shift in wavelength caused by acceleration and requires a more accurate detection system.

3.2 Photodetector Noise

Assuming a PIN photodiode is utilized, the signal-to-noise ratio (SNR) of the detection system is obtained from equation (9), where q is the electron charge, I_D is the dark current, k_B is Boltzmann's constant, T is the temperature, R_L is the load resistance, ρ is the responsivity of the photodiode, and r_I^2 is the noise level in the incident optical signal. The power that is transmitted to the photodiode, P_{pd}, is the product of the power of the light source, P_{in}, and the transmission coefficient, τ, from equation (1). Equation (9) was obtained by considering the photodiode current $\bar{I}_P = \rho P_{pd}$, shot noise $\bar{i}_S^2 = 2q(I_P + I_D)\Delta f$, thermal noise $\bar{i}_T^2 = (4k_BT/R_L)\Delta f$, amplifier noise factor F_n, and the relative intensity noise (RIN) of a laser source $\bar{i}_{RIN}^2 = I_P^2 r_I^2$ [5]:

$$SNR = \frac{(\rho\tau P_{in})^2/\Delta f}{2q(\rho\tau P_{in} + I_D) + \frac{4k_BT}{R_L}F_n + (\rho\tau P_{in} r_I)^2}. \quad (9)$$

For example, assume responsivity $1A/W$, dark current $1\mu A$, load resistance 50Ω, RIN $-120dB$, and ignore the absorption in the FPI and thermal noise in the preamplifier. For these values, the shot noise and RIN are much smaller than the thermal noise. The signal-to-noise ratio will therefore be limited mainly by the thermal noise. By setting $SNR = 1$, the noise equivalent power of the photodetector is calculated to be $18pW/\sqrt{Hz}$. If the light source is an ideal tunable laser and the wavelength is placed at the maximum slope of the transmission curve of the FPI, the minimum noise displacement can be obtained from

$$\frac{\Delta P_{pd}}{\Delta d_{min}} \approx \left[\frac{\partial P_{pd}}{\partial d}\right]_{max} = P_{in}\left[\frac{\partial \tau}{\partial d}\right]_{max}. \quad (10)$$

The noise displacement is calculated to be $0.6fm/\sqrt{Hz}$ for a reflectivity of 0.994, input power $0.1mW$, negligible absorption, zero angle of incidence, operation in air, and third order of interference. For a natural frequency of $7kHz$ this translates to an accelerometer resolution of $0.1\mu G/\sqrt{Hz}$. This is the best possible theoretical resolution, which is only obtainable for a very limited range. Note that these calculations only apply if an ideal laser and a photodiode is used. If a broadband light source and photodiode array is utilized instead, the resolution is limited by the finesse, diffraction grating, and number of elements in the photodiode array.

4 EXPERIMENTAL RESULTS

An FPI-prototype, which can potentially be used as an accelerometer, is fabricated from $450\mu m$ thick double-side polished silicon wafers by defining a membrane suspension with deep reactive ion etching (DRIE).

4.1 Fabrication Process

Fig. 4 summarizes the fabrication process. First, an antireflective coating is deposited on the backside of the polished wafer to reduce the interferometric behavior of the wafer itself. A 2000Å thick PECVD silicon nitride layer is utilized for this purpose. One of the wafers is patterned with AZ4620 photoresist and dry-etched by DRIE until a thin membrane is obtained around the cylindrical proof mass. A 400Å thick silver mirror is then deposited on top of both wafer pieces using e-beam evaporation.

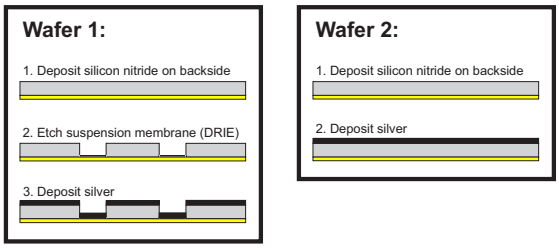

Figure 4: Fabry-Perot interferometer process flow.

4.2 Mirror Surface

Surface roughness of the silver mirrors is measured to be 64Å with an optical surface profilometer. This roughness is comparable to the 18Å specified by the manufacturer of the wafers. The defect finesse can now be calculated from equation (5). Disregarding deviations from parallelism and spherical bowing, the defect finesse due to surface roughness is $N_D = \lambda/(4.7\delta t_G) \approx 103$. Assuming the silver mirrors have a reflectivity of 0.994 [6], the reflection finesse is $N_R = \pi\sqrt{R}/(1-R) \approx 522$ according to equation (4). The effective finesse can be obtained from equation (6) and is calculated to be $N_E = 1/\sqrt{1/N_D^2 + 1/N_R^2} \approx 101$.

4.3 Assembled FPI

The two wafer pieces are placed in an alignment stage with three degrees of freedom and thin plastic spacers are put between the wafers to reduce the effects of structural vibrations when aligning the wafers. A collimating lens is used to focus the light before it is transmitted through the device. At the opposite side of the FPI another collimating lens is placed to receive the light. A single-mode optical fiber then transmits the signal to an optical spectrum analyzer, which is used to plot the intensity curves. Once aligned, slow-curing epoxy is applied between the wafers. Fig. 5 shows the fabricated wafer pieces, as well as the assembled FPI.

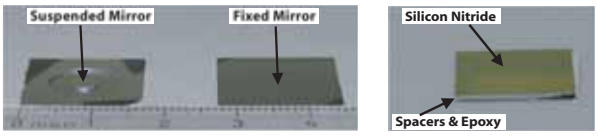

(a) (b)

Figure 5: (a) Fabricated wafers, and (b) assembled FPI.

A transmission spectrum with a free spectral range of approximately $29nm$ is displayed in Fig. 6a. Due to the low resolution and the over-sweeping of the spectrum analyzer, these peaks have been averaged and therefore look smoother than expected. In order to see the true shape of the peaks, an ELED broadband light source is used in Fig. 6b, where the FWHM of the peaks is determined to be $0.41nm$. The order of interference can be calculated as $m = \lambda/FSR \approx 53$, which means that the distance between the plates is approximately $d = m\lambda/2n \approx 41\mu m$ from equation (2). The natural frequency of the device was estimated to be $1350Hz$, yielding a resolution of $80mG$ according to equation (3). Better resolution can be achieved if the natural frequency is lowered, very flat high-reflectivity dielectric mirrors are used, and the order of interference is reduced by decreasing the cavity gap.

Defined as the FSR divided by the FWHM of the interference peaks, a finesse of $N \approx 71$ is obtained. This

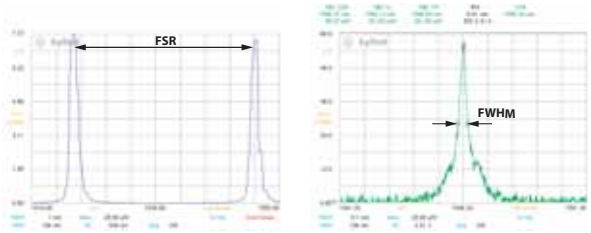

(a) (b)

Figure 6: (a) Transmission curve, and (b) FWHM of the assembled FPI.

can be compared to the estimated finesse of 101, calculated in Section 4.2. A deviation from parallelism likely accounts for the difference between the measured and estimated values. Assuming this is the only cause, the departure from parallelism is calculated to be $8.9nm$ according to equation (5).

5 CONCLUSION

It was demonstrated how the performance of FPI-based sensors depends on mechanical-thermal noise, photodetector noise, fabrication imperfections, and assembly. The main limitations are the surface quality and alignment of the mirrors. Surface roughness, curvature, or a slight deviation from parallelism will greatly reduce the finesse and in turn the resolution of the sensor. Fabrication and experimental results from a membrane-suspended FPI with silver mirrors showed that the finesse decreased by almost an order of magnitude due to surface roughness and deviation from parallelism.

This research was partially supported by UC Discovery / VIP Sensors grant 9-442531-19919-8 and NSF grant CMS-0330470.

REFERENCES

[1] M. Perez and A. Shkel, "Conceptual design and preliminary characterization of serial array system of high-resolution MEMS accelerometers with embedded optical detection," Smart Structures and Systems, 1, 63, 2005.

[2] P. Atherton, N. Reay, J. Ring and T. Hicks, "Tunable Fabry-Perot filters," Opt. Eng., 20, 806, 1981.

[3] R. Waters and M. Aklufi, "Micromachined Fabry-Perot interferometer for motion detection," Appl. Phys. Lett., 81, 3320, 2002

[4] T. Gabrielson, "Mechanical-thermal noise in micromachined acoustic and vibration sensors," IEEE Trans. Electr. Dev., 40, 903, 1993

[5] G. Agrawal, "Fiber-Optic Communication Systems," John Wiley & Sons, 156, 2002

[6] J. Bennett and E. Ashley, "Infrared Reflectance and Emittance of Silver and Gold Evaporated in Ultrahigh Vacuum," Appl. Opt., 4, 221, 1965